ISSN: 0975-766X
CODEN: IJPTFI
Available Online through *Research Article*
www.ijptonline.com

FLOW AND HEAT TRANSFER BEHAVIOUR OF NANOFLUIDS OVER A CONE SUSPENDED WITH THE NIMONIC-80A NANOPARTICLES

R.Vijayaragavan[1*] , N.Sandeep[2] , A.Thilagavathi[3]
[1,3]Department of Mathematics, Thiruvalluvar University, Vellore-632 115, India.
[2]Department of Mathematics, VIT University, Vellore-632014, Tamil Nadu, India.
Email: rvijayaraagavantvu@gmail.com

Received on: 12-02-2017 *Accepted on: 24-03-2017*

Abstract

Numerical investigation is carried out to analyze the flow and heat transfer behaviour of nanofluid caused by a rotating cone in the presence of non-uniform heat source/sink. We consider two types of base fluids namely, water and ethylene glycol embedded with Nimonic 80A nanoparticles. Nimonic 80A is a special type of heat treatable alloy with a minimum of 69% nickel and 19.5% chromium, with additives such as aluminum and titanium. With the aid of similarity transformations we reduced the governed partial differential equations as ordinary differential equations. The transformed equations are resolved numerically using R-K based shooting method. The effects of various parameters on velocity and temperature fields along with the skin friction coefficients and the local Nusselt number are discussed and presented diagrammatically. We found that the temperature field as well as the heat transfer rate of the water-Nimonic 80A nanofluid is high when compared with the EG- Nimonic 80A nanofluid.

Keywords: Nanoparticles, Nimonic 80A alloy, Irregular heat source/sink, Convection, Rotating cone.

1. Introduction

The boundary layer flow and heat transfer of nanofluids has considerable importance in industrial applications such as metal and polymer extrusion, chemical processing equipment, exchangers etc. Flow analysis plays an important role in the natural phenomena, man-made systems and also in industry. The convective heat and mass transfer over a rotating cone is important for the design of various industrial equipments like heat exchangers, canisters for nuclear waste disposal and geothermal reservoirs. In particular, Nimonic-80A is useful for manufacturing of turbine blades. It is also useful for aircraft parts, exhaust nozzles and jet engines. Due to these tremendous applications, a numerical model for three-dimensional flow due to cone at some special incidence was developed by Lin and Rubin [1]. Further, Thomas et

al. [2] proposed a finite different scheme to solve the three-dimensional boundary value problem. In continuation of this, Schiff and Steger [3] implemented an implicit finite difference scheme to solve the two dimensional boundary value problems and found that with the absence of stream wise derivatives the finite difference scheme for three-dimensional flows is approximate to two -dimensional case.

Thermophoretic suspension of particles in the gas flow due to cold surface was studied by Batchelor and Chen [4]. Eckert and Faghri [5] discussed the viscous heating of the high prandtl number fluids in the presence of temperature dependent viscosity and found that rising values of the viscous dissipation parameter enhances the temperature profiles of the flow. Magnetohydrodynamic flow in the presence of thermal radiation in a rotating fluid for unsteady case was proposed by Bestman and Adjepong [6]. Masuda et al. [7] analyzed the heat transfer characteristics of viscous fluid by suspending the ultrafine particles and found enhanced thermal conductivity of the base fluid due to the suspension of ultrafine particles. Ganapathy [8] has given a note on couettee flow in a rotating system and concluded that the increasing in rotation causes to reduce the momentum boundary layer thickness. The enhanced thermal conductivity of the base fluid by suspending the nano meter size particles was studied by Choi [9]. The heat and mass transfer in coupled hydride beds was numerically investigated by Isselhorst [10]. Singh and Singh [11] illustrated the MHD flow of dusty fluid between two parallel plates in porous medium. In this study, they concluded that increasing values of the porosity parameter enhances the thermal boundary layer thickness. An unsteady MHD flow due to non iso-thermal stretching sheet through porous medium was numerically investigated by Chamkha [12].

A review on machinability of nickel-base super alloys was illustrated by Choudhuray, and El-Bradie [13]. The diesel engine performance with air gap insulated piston was studied by Rama Mohan et al. [14]. Winstone et al. [15] discussed the advanced high-temperature materials to future aero-engines. Chakraborthy and Dutta [16] numerically investigated the heat and mass transfer in laser surface alloying in the presence of non-equilibrium solidification effects. The researchers [17-19] studied the measurement of thermal conductivity by considering different materials. Numerical investigation of heat and mass transfer in hydride hydrogen metal storage tanks for fuel cell vehicles was done by Mellouli et al. [20]. Amaranatha Reddy et al. [21-22] studied the optical properties of Mn and Cr doped nano particles. Thermal radiation effects on unsteady natural convection flow of nickel-80A nanofluid over an infinite plate were studied by Sandeep et al. [23]. In this study, they concluded that the spherical shaped nano particles have high thermal

conductivity when compared with the cylindrical shaped particles. Mallikarjuna et al. [24] analyzed the effect of chemical reaction on MHD free convective flow past a rotating cone embedded in a variable porosity regime.

Magnetohydrodynamic flow of a nanofluid with suspended dust particles in the presence of volume fraction of dust and nanoparticles was studied by Ramana Reddy et al. [25]. Heat and mass transfer in unsteady convective flow due to rotating cone or plate in a rotating fluid was numerically presented by Raju and Sandeep [26]. Jayachandra Babu et al. [27] elaborated the heat transfer characteristics of non-Newtonian nanofluid flow past a cone. Non-Newtonian bio-convection flow due to rotating cone or plate in the presence of Soret and Dufour effects was studied by Raju and Sandeep [28]. In this study, they find that the rate of heat transfer is highly significant on the flow through a rotating plate. MHD flow over a rotating cone in the presence of thermophoresis and Brownian motion effects was numerically investigated by Sulochana et al. [29] and found that thermophoresis and Brownian motion effects helps to control the thermal and concentration boundary layers. The influence of thermal radiation on magnetic ferrofluid flow past a truncated cone in the presence of irregular heat source/sink was numerically analyzed by Raju and Sandeep [30]. Phase separation in Fe–Cr–Mo ternary alloys was numerically investigated by Du et al. [31].

To the best of author's knowledge, numerical investigation of flow and heat transfer behaviour of water and ethylene glycol based Nimonic-80A alloy nanofluid due to rotating cone in the presence of irregular heat source/sink has not been reported yet. In this study, we considered two types of base fluids namely water and ethylene glycol embedded with Nimonic-80A nano particles and results are presented with the help of graphs and tables.

2. Physical model and Formulation of the problem

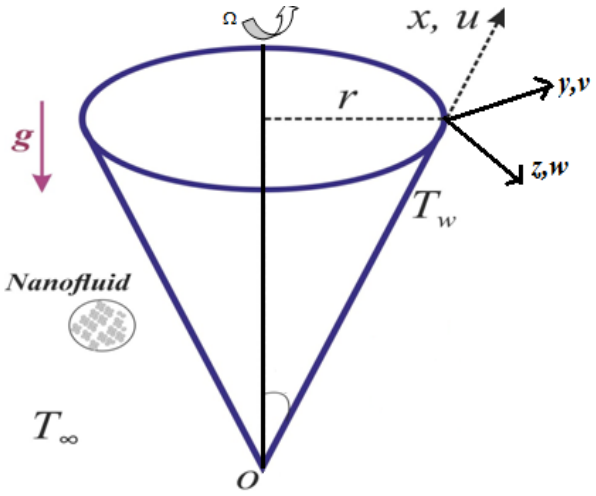

Fig.1 Physical Model of the problem.

Consider a steady, incompressible, boundary layer flow of water and ethylene glycol embedded with the Nimonic 80A alloy nano particles induced by a permeable vertical rotating cone as displayed in Fig.1. Induced magnetic field is neglected in this study. The governing boundary layer equations are as follows (See Mallikarjuna et al. [24])

Flow Analysis:

$$(rxu)_x + (rxw)_z = 0, \tag{1}$$

$$\delta^{-2}\rho_{nf}\left(uu_x + wu_z - (v^2/x)\right) = \delta^{-1}\mu_{nf}u_{zz} + g_e(\rho\beta)_{nf}(T - T_\infty)\cos\alpha, \tag{2}$$

$$\delta^{-2}\rho_{nf}\left(uv_x + wv_z + (uv/x)\right) = \delta^{-1}\mu_{nf}v_{zz}, \tag{3}$$

with the boundary conditions

$$\left.\begin{array}{l} u = 0,\ v = r\Omega,\ w = 0, \quad \text{at } z = 0, \\ u = 0,\ v = 0, \qquad\quad \text{as } z \to \infty, \end{array}\right\} \tag{4}$$

where δ is the porosity parameter, μ_{nf} is the dynamic viscosity of the nanofluid, ρ_{nf} is the nanofluid density, g_e is the acceleration due to gravity, β_{nf} is the volumetric expansion of the nanofluid due to the temperature differences. To obtain the nonlinear differential equations for momentum, we now introducing the following non-dimensional

$$\left.\begin{array}{l} \eta = \sqrt{\dfrac{\Omega\sin\alpha}{v^{1/2}}}z, u = x\Omega\sin\alpha\, f(\eta), v = x\Omega\sin\alpha\, g(\eta), r = x\sin\alpha, \\ w = \sqrt{v_f\Omega\sin\alpha}\,h(\eta), \theta(\eta) = \dfrac{T - T_\infty}{T_w - T_\infty}, T_w(x) - T_\infty = \dfrac{(T_L - T_\infty)x}{L}, \end{array}\right\} \tag{5}$$

The nanofluid constants are given by

$$(\rho\beta)_{nf} = (1-\phi)(\rho\beta)_f + \phi(\rho\beta)_s,\ (\rho c_p)_{nf} = (1-\phi)(\rho c_p)_f + \phi(\rho c_p)_s,$$

$$\frac{k_{nf}}{k_f} = \frac{(k_s + 2k_f) - 2\phi(k_f - k_s)}{(k_s + 2k_f) + \phi(k_f - k_s)},\quad \mu_{nf} = \frac{\mu_f}{(1-\phi)^{2.5}},\quad \rho_{nf} = (1-\phi)\rho_f + \phi\rho_s \tag{6}$$

where L is the slant height of the cone, T_L is the surface temperature of the cone at the base $(x = L)$ and ϕ is the nano particle volume fraction. The subscripts f and s refer to fluid and solid fraction properties respectively.

Using equations (5) and (6), the equations (1) to (3) transformed to

$$f = -\frac{1}{2}h', \tag{7}$$

$$-\frac{\delta^{-1}}{(1-\phi)^{2.5}}h'''+\delta^{-2}\left((1-\phi)+\phi\left(\frac{\rho_s}{\rho_f}\right)\right)\left(hh''+\left(-\frac{1}{2}h'^2+2g^2\right)\right)+2\Lambda\left((1-\phi)+\phi\left(\frac{(\rho\beta)_s}{(\rho\beta)_f}\right)\right)\theta\cos\alpha=0, \quad (8)$$

$$-\frac{\delta^{-1}}{(1-\phi)^{2.5}}g''-\delta^{-2}\left((1-\phi)+\phi\left(\frac{\rho_s}{\rho_f}\right)\right)(hg'-h'g)=0, \quad (9)$$

with the transformed boundary conditions

$$\left.\begin{aligned} h'=0, g=1, \quad & at \ \ \eta=0, \\ h'=0, g=0, \quad & as \ \ \eta\to\infty, \end{aligned}\right\} \quad (10)$$

where $\Lambda=\dfrac{g_e\beta_f(T_w-T_\infty)L^3}{\nu_f^2}$ is the dimensionless thermal buoyancy parameter.

Heat Transfer analysis:

The boundary layer energy equation in the presence irregular heat source/sink is given by

$$uT_x+wT_z=\left(k_{nf}/(\rho c_p)_{nf}\right)T_{zz}+\left(k_f u(x)/x\nu_f(\rho c_p)_{nf}\right)\left(A^*(T_w-T_\infty)f'+B^*(T-T_\infty)\right), \quad (11)$$

with the boundary conditions

$$T=T_w(x), \ \text{at} \ z=0, \ T=T_\infty, \ \text{as} \ \ z\to\infty, \quad (12)$$

where T is the fluid temperature, T_w, T_∞ are the temperature of the fluid near the surface and ambient, k_{nf} is the effective thermal conductivity of the nanofluid, $(c_p)_{nf}$ is the specific heat at constant pressure. Using similarity transforms of (5) and (6), the equation (11) reduced to

$$\frac{k_{nf}}{k_f}\theta''+\left(A^*f'+B^*\theta\right)-\Pr\left(1-\phi+\phi\left(\frac{(\rho c_p)_s}{(\rho c_p)_f}\right)\right)\left(h\theta'-\frac{1}{2}h'\theta\right)=0, \quad (13)$$

with the transformed boundary conditions

$$\theta=1, \ \text{at} \ \eta=0, \theta=0, \ \text{as} \ \ \eta\to\infty, \quad (14)$$

where $\Pr=k_f/(\rho c_p)_f$, is the Prandtl number, positive values of A^*, B^* corresponds to heat generation and negative values are corresponds to heat absorption.

For physical quantities of interest the friction factors along x, y directions and local Nusselt number are given by

$$C_{fx}\,\mathrm{Re}^{1/2}=-h''(0), \mathrm{Re}^{1/2}\,C_{fy}=-(1/2)g'(0), \mathrm{Re}^{-1/2}\,Nu_x=-(k_{nf}/k_f)\theta'(0), \quad (15)$$

where $\mathrm{Re} = x^2\Omega\sin\alpha/\nu_f$, is the Reynolds number.

3. Results and Discussion

The set of nonlinear ordinary differential equations (7)-(9) and (13) subjected to the boundary conditions (10) and (14) have been solved numerically using R-K-Felhberg integration scheme. Results depict the influence of non-dimensional governing parameters on velocity, temperature fields along with the friction factors and local Nusselt number. For numerical computations we considered the non-dimensional parameter values as $\phi = A^* = B^* = 0.1$, $\delta = 10, \Lambda = 20, \alpha = \pi/4$. These values are kept as common in entire study except the varied values in respective figures and tables. In graphical results $f(\eta), g(\eta)$ and $h(\eta)$ represents tangential, circumferential and normal velocities and $\theta(\eta)$ represents the temperature profiles of the flow. Table 1 shows the thermophysical properties of water, ethylene glycol and Nimonic 80A nano particles.

Table 1. Thermophysical properties of water, ethylene glycol and Nimonic 80A nano particles.

Physical properties	Water	EG	Nimonic-80A
$c_p(J/KgK)$	4179	2386	448
$\rho(Kg/m^3)$	997.1	1115	8152
$k(W/mK)$	0.613	0.252	112
$\beta\times10^{-5}/K$	21	57	1.27

Figs. 2-5 depict the influence of volume fraction of Nimonic 80A alloy nanoparticles on velocity and temperature fields. It is evident that increasing values of volume fraction of nanoparticles suppress the velocity profiles in a tangential direction. But we have seen reverse profiles in normal and circumferential velocity fields. It is interesting to note here that the momentum boundary layer of water-Nimonic 80A nanofluid is highly influenced by change in the volume fraction of nanoparticles. It can also be observed that the increasing value of volume fraction of nanoparticles effectively enhances the thermal boundary layer thickness of both the nanofluids. From Fig. 5, it is clear that the temperature profile of water-Nimonic 80A nanofluid is significantly enhanced for rising values of ϕ. This leads to the conclusion that the thermal conductivity of water-based Nimonic 80A is highly effective when compared with the EG-Nimonic 80A.

Figs. 6-9 illustrate the effect of thermal buoyancy parameter on velocity and temperature profiles of the flow. It is observed that the rising values of the buoyancy parameter enhances the tangential, circumferential velocity profiles and declines the normal velocity field. Generally, increasing values of the buoyancy parameter develops the acceleration in the flow. These causes to develop the momentum boundary layer in tangential and circumferential directions. It is also observed that the rising values of buoyancy parameter depreciate the temperature fields of both nanofluids. In particular, EG-Nimonic 80A is highly influenced by buoyancy parameter.

The effect of porosity parameter on velocity and temperature fields is displayed in Figs. 10-13. It is clear that, increasing values of the porosity parameter declines the velocity profiles in both tangential and circumferential direction. Reverse behaviour has been observed for the normal velocity profiles and temperature field. Physically, rising values of the porosity parameter develops the internal heat energy to the flow and hence the thermal boundary layer thickness. It is also observed that the water-based Nimonic 80A nanofluid is highly influence by the increasing values of the porosity parameter. Figs. 14 and 15 show the effect of irregular heat source/sink parameters on temperature profiles of the flow. We observed an interesting result that increasing values of A^* enhances the temperature profiles of both nanofluids near the boundary and shows the reverse action at free stream. We have noticed a similar type of results for rising values of B^*. Physically, positive values of non-uniform heat source/sink parameters acts like heat producers, this helps to boost up the thermal boundary layer of the flow.

It s also observed that EG-Nimonic 80A nanofluid has less influenced by the increasing values of B^*. Table 2 depicts the effect of non-dimensional parameters on friction factors and the local Nusselt number for water and EG-based Nimonic 80A nanofluids. It is evident that the increasing values of volume fraction of nanoparticles and porosity parameter depreciate the friction factors along with the heat transfer rate for both nanofluids. The rising values of thermal buoyancy parameter effectively enhance the skin friction coefficients and the local Nusselt number. Increasing values of the irregular heat source/sink parameters helps to increase the friction factor in normal direction and declines the wall friction in circumferential direction. It is also observed a fall in heat transfer rate due to the increasing values of irregular heat source/sink parameters. Table 3 illustrates the validation of the present study by comparing with the existed literature. We found a good agreement of the present results by comparing with the published results under some special limited cases.

Table 2. Variation in friction factors, local Nusselt and Sherwood numbers for different values of non-dimensional governing parameters.

Nimonic 80A +	ϕ	δ	Λ	A^*	B^*	$-h''(0)$	$-g'(0)$	$-\theta'(0)$
EG	0.1					10.358661	0.054451	8.763727
	0.2					8.559139	0.065846	7.906082
	0.3					6.994443	0.077705	7.110544
Water	0.1					10.350259	0.050422	2.554869
	0.2					8.563232	0.061640	2.294713
	0.3					7.013243	0.073882	2.054395
EG		10				10.358661	0.054451	8.763727
		12				8.910115	0.092074	8.335430
		14				7.754497	0.107444	7.958583
Water		10				10.350259	0.050422	2.554869
		12				8.914739	0.090268	2.434556
		14				7.764455	0.106495	2.327681
EG			15			7.886099	0.072942	8.002543
			20			10.358661	0.054451	8.763727
			25			12.769368	0.035258	9.395942
Water			15			7.885565	0.070028	2.338812
			20			10.350259	0.050422	2.554869
			25			12.751146	0.030022	2.732870
EG				0		1.388303	0.999870	4.289996
				10		1.388406	0.999870	3.688810
				20		1.388509	0.999870	3.087666
Water				0		1.416430	0.999860	1.277561
				10		1.417577	0.999860	0.430336
				20		1.418710	0.999860	-0.416357

EG					0	1.388301	0.999870	4.290769
					4	1.388409	0.999870	4.014403
					8	1.388495	0.999870	3.800075
Water					0	1.416306	0.999860	1.290604
					4	1.423497	0.999860	0.248735
					8	1.433179	0.999859	-0.966697

Table 3 Comparison of the present results for skin friction coefficient and local Nusselt number when $\Pr = 0.7, Da^{-1} = \Gamma = Sc = \gamma = M = \phi = 0$

Λ	Mallikarjuna et al. [24] $-g'(0)$	Present Results $-g'(0)$	Mallikarjuna et al. [24] $-\theta'(0)$	Present Results $-\theta'(0)$
0	0.61583	0.615830	0.42842	0.428416
0.1	0.65492	0.654931	0.46141	0.461411
1.0	0.85080	0.850802	0.61213	0.612121
10	1.40363	1.403625	1.01748	1.017480

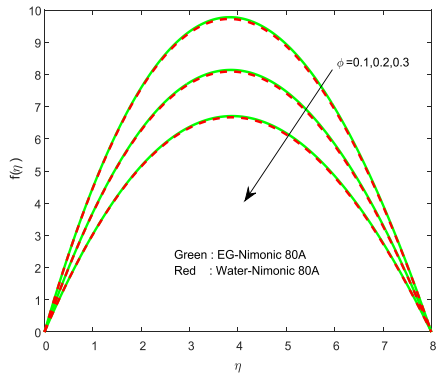

Fig.2 Tangential velocity field for ϕ

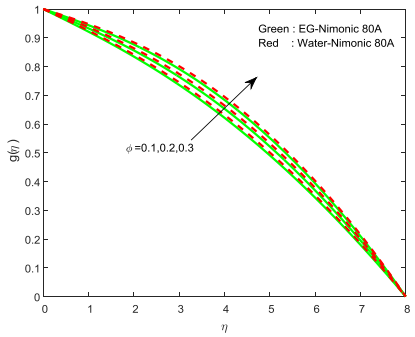

Fig.3 Circumferential velocity field for ϕ

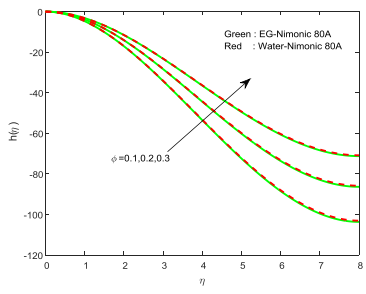

Fig.4 Normal velocity field for ϕ

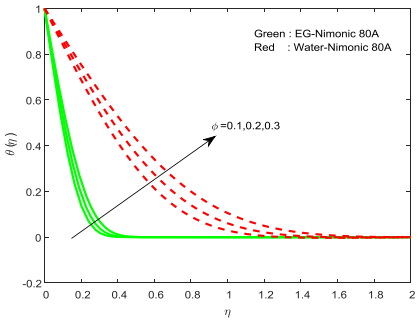

Fig.5 Temperature field for ϕ

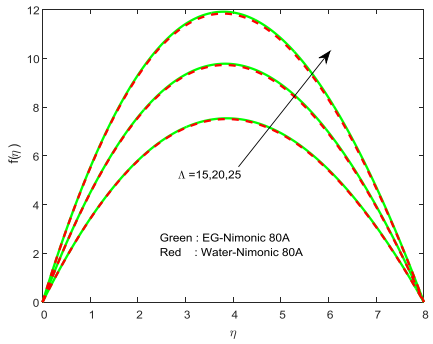

Fig.6 Tangential velocity field for Λ

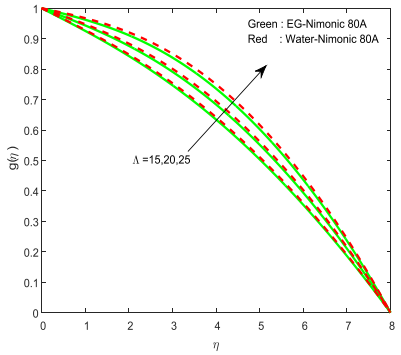

Fig.7 Circumferential velocity field for Λ

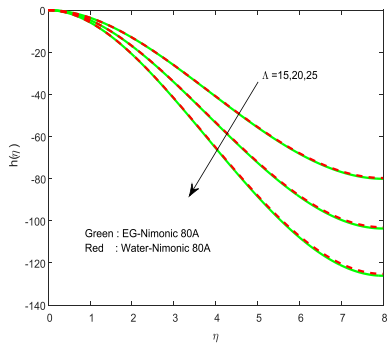

Fig.8 Normal velocity field for Λ

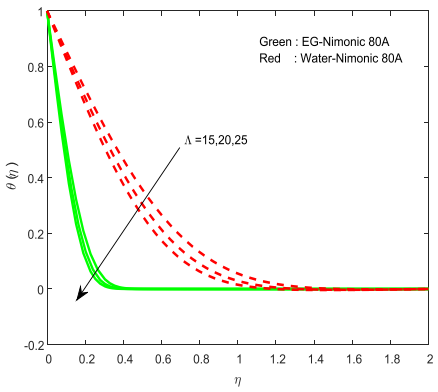

Fig.9 Temperature filed for Λ

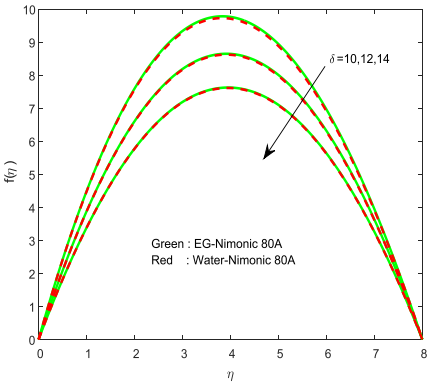

Fig.10 Tangential velocity field for δ

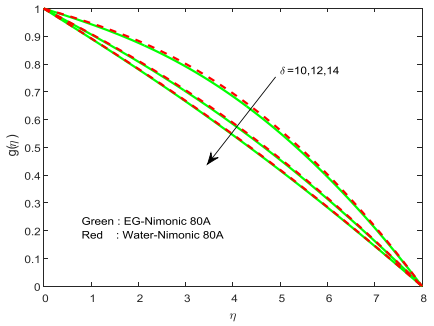

Fig.11 Circumferential velocity field for δ

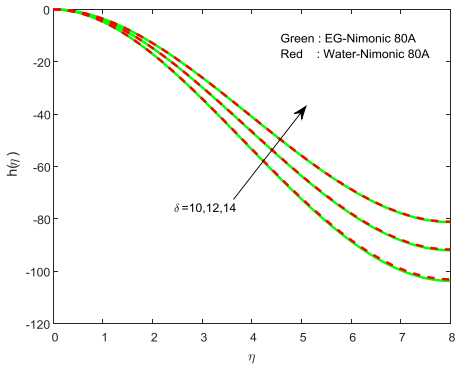

Fig.12 Normal velocity field for δ

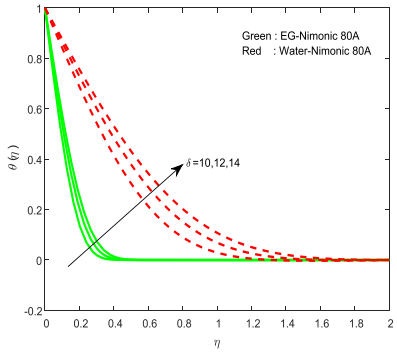

Fig.13 Temperature field for δ

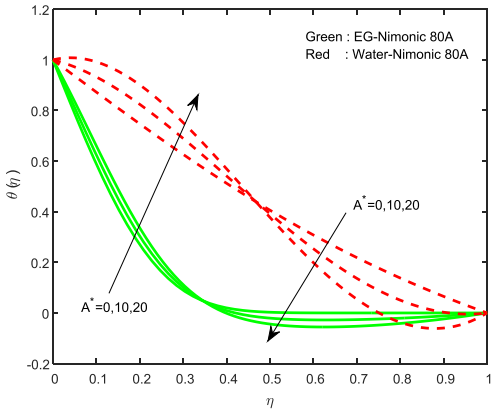

Fig.14 Temperature field for A^*

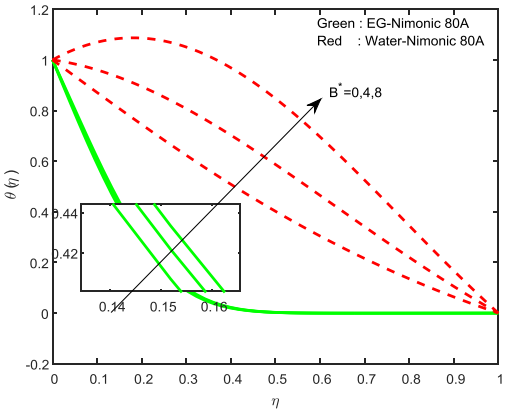

Fig.15 Temperature filed for B^*

4. Conclusions

This study presents dual solutions for the flow and heat transfer behaviour of water and ethylene glycol based Nimonic-80A alloy due to rotating cone in the presence of irregular heat source/sink. The conclusions of the present study are as follows:

- Rise in the thermal buoyancy parameter enhances the heat transfer rate of both water-Nimonic 80A and EG-Nimonic 80A nanofluids.
- The momentum boundary layer of the normal velocities is unique for both nanofluids.
- The heat transfer performance of the Water-Nimonic 80A nanofluid is significantly high when compared with the -Nimonic 80A nanofluid.
- Irregular heat source/sink parameters have tendency to control the thermal boundary layer of both nanofluids.
- The circumferential velocity field of water-Nimonic 80A nanofluid is high when compared with the EG-Nimonic 80A nanofluid.

References

1. T. C. Lin, S. G. Rubin, Viscous flow over a cone at moderate incidence-1, Hypersonic tip region, Computers & Fluids 1 (1973) 37-57.
2. P. D. Thomas, M. Vinokur, R. A. Bastianon and R. J. Conti, Numerical solution for three-dimensional inviscid supersonic flow, AIAA Journal 10(7) (1972) 887-894.

3. L. B. Schiff, J. L. Steger, Numerical simulation of steady supersonic viscous flow, AIAA Journal 18(12) (1980) 1421-1430.
4. G.K. Batchelor, C. Chen, Thermophoretic deposition of particles in gas flowing over cold surface, Journal of Colloid Interface Science, 35 (1985) 21-37.
5. E.R.G. Eckert, M.Faghri, Viscous heating of high Prandtl number fluids with temperature-dependent viscosity, Int'l Journal of Heat and Mass Transfer 29 (1986) 1177–1183.
6. A.R.Bestman, S.K.Adjepong, Unsteady hydromagnetic free-convection flow with radiative heat transfer in a rotating fluid, Astrophysics and Space Science, 143 (1988) 73-80.
7. H.Masuda, A.Ebata, K.Teramae and N.Hishinuma, Alteration of thermal conductivity and viscosity of liquid by dispersing ultrafine particles, Netsu Bussei, 7(4) (1993) 227-233.
8. R.Ganapathy, A note on oscillatory couettee flow in a rotating system, Journal of Applied Mechanics, 61 (1994) 205-209.
9. S.U.S.Choi, Enhanced thermal conductivity of nanofluids with nano particles, development and applications of Newtonian flows. FED. vol.231/MD-vol.66 (1995) 99-105.
10. A.Isselhorst, Heat and mass transfer in coupled hydride reaction beds, J. Alloys and Compounds, 231 (1995) 871-879.
11. A.K. Singh and N.P. Singh, MHD flow of a dusty visco-elastic liquid through a porous medium between two inclined parallel plates, Proceeding of national academy of science India, 66(A) (1996) 143-150.
12. A.J. Chamkha, Unsteady hydromagnetic flow and heat transfer from a non-isothermal stretching sheet immersed in a porous medium, International Communications in Heat and Mass Transfer 25 (1998) 899–906.
13. I.A.Choudhuray, M.A.El-Bradie, Machinability of nickel-base super alloys: a general review, J. Materials processing Tech., 77 (1998) 278-284.
14. K.Rama Mohan, C.M.Varaprasad, M.V.S. Murali Krishna, Performance of a Low Heat Rejection Diesel Engine With Air Gap Insulated Piston, J.Eng. Gas Turbines Power 121 (1999) 530-539.

15. M.R.Winstone, A.Partridge, J.W.Brooks, The contribution of advanced high-temperature materials to future aero-engines, Proceedings of the Institution of Mechanical Engineers, Part L: Journal of Materials: Design and Applications, 215 (2001) 63-73.
16. S.Chakraborthy, P.Dutta, Numerical modeling of heat and mass transfer in laser surface alloying: non-equilibrium solidification effects, Materials and Manufacturing Processes, 17 (2002) 455-468.
17. I.L.Ferreira, A.Garcia, B.Nestler, On macrosegregation in ternary Al–Cu–Si alloys: numerical and experimental analysis, Scripta Materilia, 50 (2004) 407-411.
18. J.C.Tan, S.A.Tsipas, I.O.Golosnoy, J.A.Curran, S.Paul, T.W.Clyne, A steady-state Bi-substrate technique for measurement of the thermal conductivity of ceramic coatings, Surface and coatings technology, 201 (2006) 1414-1420.
19. P. Muthukumar, S.Venkata Ramana, Numerical simulation of coupled heat and mass transfer in metal hydride-based hydrogen storage reactor, J. Alloys and Compounds, 472 (2009) 466-472.
20. [20] S.Mellouli, F.Askri, H.Dhaou, A.Jemni, S.Ben Nasrallah, Numerical simulation of heat and mass transfer in metal hydride hydrogen storage tanks for fuel cell vehicles, Int.J.Hydrogen Energy, 35 (2010) 1693-1705.
21. D. Amaranatha Reddy, A. Divya, G. Murali, R.P. Vijayalakshmi, B.K. Reddy, Synthesis and optical properties of Cr doped ZnS nanoparticles capped by 2-mercaptoethanol, Physica B: Condensed Matter, 406 (2011) 1944-1949.
22. D. Amaranatha Reddy, S. Sambasivam, G. Murali, B. Poornaprakash, R.P. Vijayalakshmi, Y. Aparna, B.K Reddy, J.L. Rao, Effect of Mn co-doping on the structural, optical and magnetic properties of ZnS: Cr nanoparticles, Journal of Alloys and Compounds, 537 (2012) 208-2015.
23. N.Sandeep, V.Sugunamma, P.Mohan Krishna, Effects of Radiation on an Unsteady Natural Convective Flow of a EG-Nimonic 80a Nanofluid Past an Infinite Vertical Plate, Advances in Physics Theories and Applications, 23 (2013) 36-43.
24. B. Mallikarjuna, A. M. Rashad, Ali J. Chamkha, S. Hariprasad Raju, Chemical reaction effects on MHD convective heat and mass transfer flow past a rotating vertical cone embedded in a variable porosity regime, Afrika Mathematika, DOI 10.1007/s13370-015-0372-1.

25. J.V.Ramana Reddy, N.Sandeep, V.Sugunamma, MHD Flow of a Nanofluid Embedded with Dust Particles Due to Cone with Volume Fraction of Dust and Nano Particles, Procedia Engineering, 127 (2015) 1026-1033.
26. C.S.K.Raju, N.Sandeep, Dual solutions for unsteady heat and mass transfer in bio-convection flow towards a rotating cone/plate in a rotating fluid, Int.J.Eng. Resaech in Afrika, 20 (2015) 161-176.
27. M.Jayachnadra Babu, N.Sandeep, C.S.K.Raju, Heat and mass transfer in MHD Eyring-Powell nano fluid flow due to cone in porous medium, Int.J.Eng. Resaech in Afrika, 19 (2015) 57-74.
28. C.S.K.Raju, N.Sandeep, Heat and mass transfer in MHD non-Newtonian bio-convection flow over a rotating cone/plate with cross diffusion, Journal of Molecular Liquids 215 (2016) 115–126.
29. C.Sulochana, G.P.Ashwin Kumar, N.Sandeep, Numerical investigation of chemically reacting MHD flow due to a rotating cone with Thermophoresis and Brownian motion, Int.J. Advanced Science and Technology, 86 (2016) 61-74.
30. C.S.K.Raju, N.Sandeep, The effect of thermal radiation on MHD ferrofluid flow over a truncated cone in the presence of non-uniform heat source/sink. Global Journal of Pure and Applied Mathematics, 12(1) (2016) 9-15.
31. L.Du, L.Wang, B.Zheng, H.Du, Numerical simulation of phase separation in Fe–Cr–Mo ternary alloys, J. Alloys and Compounds, 663 (2016) 243-248.